Applied Catalysis B: Environmental 100 (2010) 10–18

Contents lists available at ScienceDirect

Applied Catalysis B: Environmental

journal homepage: www.elsevier.com/locate/apcatb

Review

A global description of DOC kinetics for catalysts with different platinum loadings and aging status

K. Hauff*, U. Tuttlies, G. Eigenberger, U. Nieken

Insitute for Chemical Process Engineering, University Stuttgart, Böblinger Str. 78, 70199 Stuttgart, Germany

ARTICLE INFO

Article history:
Received 3 February 2010
Received in revised form 23 July 2010
Accepted 28 July 2010
Available online 6 August 2010

Keywords:
DOC
Aging
Global kinetic model
Simulation
Kinetic measurement

ABSTRACT

Global kinetic models usually require a recalibration in case of catalyst aging or changes in the precious metal loading. In this contribution the lean oxidation kinetics of CO, propene and NO for five (Pt-γ-Al_2O_3) diesel oxidation catalysts (DOCs) with different platinum loadings and stages of aging are determined from isothermal steady-state experiments. HR-REM shows that for all catalysts the platinum particles have diameters larger than 8 nm, so that the catalysts are in the structure insensitive regime. It will be confirmed that in this case the catalytic activity is only proportional to the catalytically active surface which can be determined easily by CO-chemisorption experiments. In order to model the CO- and propene-oxidation kinetics for differently aged and platinum loaded catalyst, only one parameter, the catalytically active surface, has to be changed in the global kinetic models. The same is true for NO oxidation at higher temperatures, where platinum stays in an oxidized state.

Contents

1. Introduction

Diesel oxidation catalysts (DOCs) are nowadays a standard device in exhaust aftertreatment. In most applications DOCs are combined with diesel particle filters (DPF) and either nitrogen oxides storage catalysts (NSCs) or selective catalytic reduction (SCR) catalysts. A correct prediciton of the DOC con-

* Corresponding author. Tel.: +49 711 685 85245; fax: +49 711 685 85242.
E-mail address: karin.hauff@icvt.uni-stuttgart.de (K. Hauff).

0926-3373/$ – see front matter © 2010 Elsevier B.V. All rights reserved.
doi:10.1016/j.apcatb.2010.07.036

Nomenclature

a_i^j	exponent of the mole fraction in the inhibition term
A_{geo}	geometric surface (m^2)
a_{geo}	specific geometric surface (m^2/m^3)
c_p^b	specific heat capacity of gas phase (J/Kg K)
c_p^s	specific heat capacity of solid phase (J/Kg K)
D_{bulk}	diffusion coefficient in the gas bulk (m^2/s)
E_a	activation energy (J/mol)
$\Delta h_{R,i}$	reaction enthalpy of reaction i (J/mol)
k_i	reaction rate constant of reaction i (mol/m^2 s)
K_i^{inhj}	inhibition term constant of component j in reaction i
I_i	inhibition term of reaction i
m_{Pt}	mass of platinum (kg)
MW_{Pt}	molecular weight of platinum (g/mol)
n_{Pt}^{surf}	accessible platinum atoms
n_{Pt}^{total}	all platinum atoms
O_{Pt}	specific platinum surface
q_i^j	exponent of the mole fraction
r_i	reaction rate of reaction i (mol/m^2 s)
T	temperature (K)
v^b	bulk velocity (m/s)
y_j^b	mole fraction of component j in the bulk
y_j^s	mole fraction of component j at the surface

Greek letters

α	heat transfer coefficient (W/m^2 K)
β_j	mass transfer coefficient (m/s)
Γ_{Pt}	surface site density (mol/cm^2)
ε_b	open frontal area
$\nu_{i,j}$	stoichiometric coefficient
λ_b	thermal conductivity of gas phase (W/m K)
λ_s	thermal conductivity of solid phase (W/m K)
ρ_b	density of gas phase (kg/m^3)
ρ_s	density of solid phase (kg/m^3)

version is crucial for the simulation of the whole aftertreatment system.

Large efforts have been made to develop appropriate simulation models for automotive catalysts [1–5]. Since the CO, HC and NO_x conversion of DOCs is significantly affected by the precious metal loading and the aging status of the catalyst, global kinetic models require a recalibration of the reaction kinetics if the precious metal loading or its dispersion is changed. Some models include the catalytic surface area as an independent variable in the reaction rate term, which allows the predicition of catalyst performance with different precious metal loadings [6–8]. However there is no comprehensive experimental proof, whether scaling of rate expressions by catalytic surface area is practicable.

In this paper, the well known approach is presented and verified which assumes, that the reaction rate is directly proportional to the catalytically active platinum surface, which can be determined by CO chemisorption. This enables us to accurately predict the catalyst performance of aged or of differently loaded catalysts with a single additional parameter.

The work consists of an experimental and a theoretical part. For the experiments model catalysts with specified precious metal loading were hydrothermally aged and characterized regarding their precious metal dispersion, particle diameters and conversion behaviour. On the basis of generalized Langmuir–Hinshelwood kinetics, it is shown that the linear correlation with the catalytic surface area is valid for different precious metal loadings and for different aging states.

Table 1
Catalysts.

Name	Precious metal loading (g/ft^3)	Aging temperature (°C)
DOC120	130.06	700
DOC120-850	127.8	850
DOC120-950	129.97	950
DOC60	58.37	700
DOC20	22.51	700

2. Experiments

2.1. Aging

The catalysts (Pt-g-Al_2O_3, 400 cpsi monolith) have been manufactured by a commercial catalyst supplier with three different platinum loadings as shown in Table 1.

The catalysts for the study of precious metal loading variation (DOC20, DOC60 and DOC120) were hydrothermally pretreated for 16 h at 700 °C. For the variation of the aging status two DOC120 samples were hydrothermally aged for 16 h at 850 °C (DOC120-850) and at 950 °C (DOC120-950). For pretreatment/aging in the furnace, the monoliths (diameter 75 mm and length 125 mm) were canned and flowed through with 10% water in air. After aging the monoliths are divided in catalyst slices (30 mm × 40 mm, one channel height = 1.4 mm) for kinetic measurements and cylindrical samples (diameter 19.5 mm and length 35 mm) for the characterization.

2.2. Kinetic measurements

Steady-state experiments were carried out under lean conditions in an isothermal flat bed reactor (Fig. 1) under realistic flow conditions with synthetic exhaust gas [9]. The reactor consists of a bottom and a top shell, made from stainless steel, and thermostated by heating cartridges. Five slices of a monolith catalyst (30 mm × 40 mm, one channel height) are placed in the groove of the bottom shell behind one inert slice for gas preheating and uniform flow distribution. As the thin slices are surrounded by massive metal shells, which provide high thermal mass, the catalyst is isothermal despite the heat release of exothermal reactions. A thermocouple is placed in the middle of each catalyst slice to ensure isothermal conditions. Lateral withdrawls after each slice allow the measurement of the concentration profiles along the catalyst length. Gas analysis was accomplished with SI-mass spectroscopy (MS4). The synthetic exhaust gas (SV = 40,000 h^{-1}) consisted of 12%O_2, 7%CO_2, 10%H_2O and varying concentrations of C_3H_6 (0–1000 ppm), CO (0–15,000 ppm) and NO (0–500 ppm). Nitrogen was used for balance. The temperature varied between 120 and 450 °C.

2.3. Catalyst characterization

The platinum particle size distribution was obtained by analysis of HR-REM images, provided by ITCP, Karlsruhe.

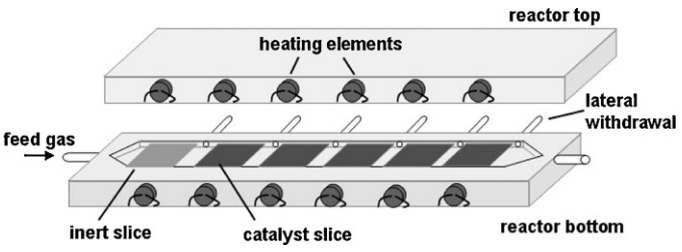

Fig. 1. Sketch of the isothermal flat bed reactor.

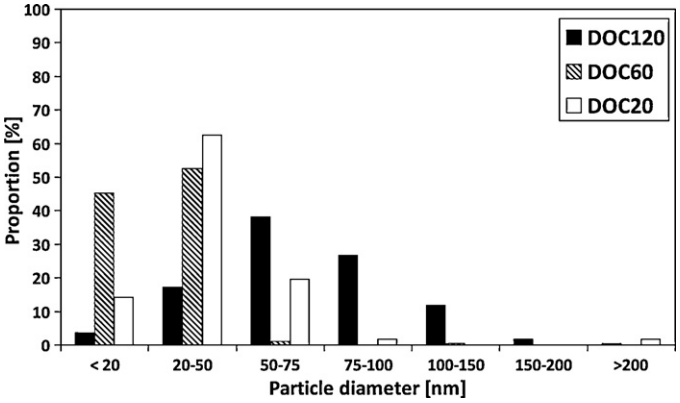

Fig. 2. Particle size distribution of precious metal variation.

To determine the catalytically active surface, CO-chemisorption measurements [10] were carried out at ITCP, University Karlsruhe. The catalyst was first reduced with 10% H_2 in helium at 400 °C for 16 h and then heated up to 600 °C in pure helium. After cooling down, the metal surface was exposed to 5% CO at room temperature for 1 h. During a fast temperature ramp the CO was desorbed. The amount of desorbed CO is equal to the amount of accessible platinum surface sites n_{Pt}^{surf}. Herewith the platinum dispersion D can be calculated as well as the specific platinum surface O_{Pt} which is the ratio of catalytic active surface to geometric surface.

$$D = \frac{n_{Pt}^{surf}}{n_{Pt}^{total}}; \qquad O_{Pt} = D\frac{m_{Pt}}{MW_{Pt}\Gamma_{Pt}A_{geo}} \tag{1}$$

3. Results of catalyst characterization

The particle size characterization showed that the platinum particles of DOC120 are between 15 and 250 nm in diameter (Fig. 2). The smallest particles for DOC20 were about 8 nm, for DOC60 about 10 nm. Since DOC60 was prepared in a different way, the particle size distribution is more narrow.

The particle size distribution after hydrothermal aging at 850 °C (DOC120-850) shows an increase in small particles as well as large particles (Fig. 3). This leads to the assumption that the particles undergo Ostwald ripening [11]. At elevated temperatures the platinum on the catalysts sinter by atomic migration [12]. Small particles lose platinum atoms which are taken up by big particles. Therefore DOC120-850 has more particles in the classes between 150 and 500 nm as DOC120 but also more in the range between 20 and 75 nm and as a consequence less in the medium particle size classes. For DOC120-950 the process of Ostwald ripening is already

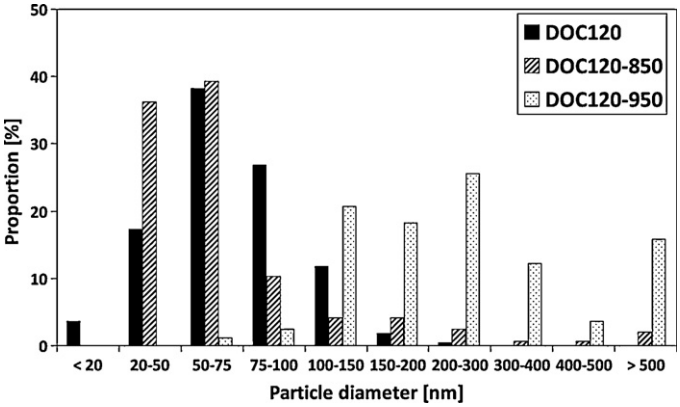

Fig. 3. Particle size distribution of aged catalysts.

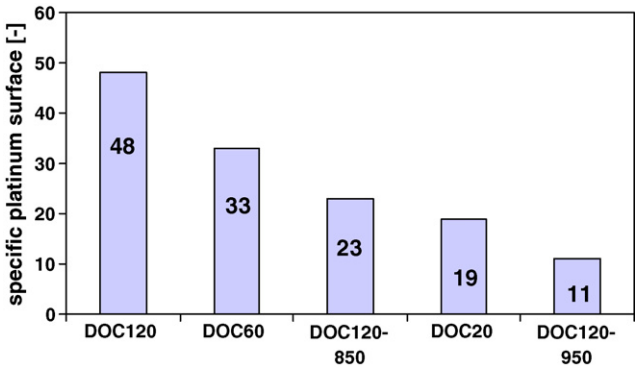

Fig. 4. Specific platinum surface measured by chemisorption (ITCP University Karlsruhe).

finished, the small particles have disappeared and the whole distribution has been shifted to higher diameters. The aged catalysts have no particles smaller than 20 nm.

The specific platinum surface is determined by chemisorption measurements (see Section 2.3). In Fig. 4 the specific platinum surface is shown for the five investigated catalysts. For the aged catalysts (DOC120-850 and DOC120-950) it is smaller because sintering decreases the platinum surface. For the catalysts with reduced platinum loading (DOC60 and DOC20) the measurement showed smaller specific platinum surfaces as well.

4. Catalyst model

In the following, a standard model for DOCs is presented. The kinetic expressions, accounting for precious metal variation or aging, will be discussed in Section 5.

The mathematical model is a one dimensional convection diffusion model for gas (Eq. (2)) and solid phase (Eq. (3)). Gaseous species are denoted y_j^b, species at the washcoat surface y_j^s. Both phases are connected by mass transfer terms. Sherwood number correlations are used to calculate the external mass transfer coefficients β_j. The influence of internal mass transfer resistances in the washcoat is included in the global kinetics. The reaction rates are based on Langmuir–Hinshelwood kinetics [5] and will be described in Section 6.

$$\frac{\partial y_j^b(x,t)}{\partial t} = -v^b\frac{\partial y_j^b(x,t)}{\partial x} + D_{bulk}\frac{\partial^2 y_j^b(x,t)}{\partial x^2} - a_{geo}\beta_j(y_j^b(x,t) - y_j^s(x,t)) \tag{2}$$

$$0 = \beta_j\cdot(y_j^b(x,t) - y_j^s(x,t)) + \frac{RT}{p}\sum_{i=1}^{I^S}(\nu_{i,j}r_i^s(y_j^s)) \tag{3}$$

For simulation of the adiabatic light-off experiments, the heat balance is taken into account. The heat balance of the gas phase covers concevtion, heat transfer to the solid phase and axial heat conduction:

$$\varepsilon_b c_p^b\rho_b\frac{\partial T^b(x,t)}{\partial t} = -\varepsilon_b c_p^b\rho_b v^b\frac{\partial T^b}{\partial x} + a_{geo}\alpha(T^{sol} - T^b) + \varepsilon_b\lambda_b\frac{\partial^2 T^b}{\partial x^2} \tag{4}$$

The heat balance of the solid phase accounts for axial heat conduction, heat transfer to the gas phase and heat release by reaction:

$$(1-\varepsilon_b)\rho_s c_p^s\frac{\partial(T^{sol}(x,t))}{\partial t} = (1-\varepsilon_b)\lambda_s\frac{\partial^2 T^{sol}}{\partial x^2} - a_{geo}\alpha(T^{sol} - T^b) + a_{geo}\sum_{i=1}^{I}(-\Delta h_{R,i})r_i \tag{5}$$

The model equations have been implemented in the simulation software PREDICI. The parameter estimation is accomplished by a least squares fit by newton method.

5. Structure sensitivity/insensitivity

The parameters of a global kinetic model are derived by fitting to experimental data. If the catalytic surface area is included as an independent variable, it allows the predicition of catalyst performance with different precious metal loadings [7,8]. This will be confirmed later in this paper by studying a variation of precious metal loading. Furthermore it will be shown that it is valid for hydrothermally aged catalysts as well.

However, it should be mentioned that this is subject to constraints. The direct correlation of the catalytic actvity with the catalytic surface area is only valid, if the reaction is structure insensitive. If a reaction shows a dependence of the activity with the particle diameter, the reaction is structure sensitive. Structure sensitivity originates from the fact that platinum particles exhibit different types of surface sites on which the reactions show different turn over frequencies. Since the ratio of different surface sites changes with the particle diameter, the overall conversion rates can vary with the particle diameter. If the particle diameter exceeds a critical value, the ratio of planar faces to edges and corners does barely change [13,14]. In this case, the reaction is considered structure insensitive. For CO oxidation on platinum the literature results can be classified in three groups [15]:

- particle diameter $\gg$ 2.5 nm under stoichiometric reaction conditions: the TOF is independent of particle size.
- 1–6 nm under stoichiometric reaction conditions: TOF changes only little with particle size.
- <2 nm: structure sensitive under both CO-rich and CO-lean conditions.

Thus, the correlation of the catalytic actvity with the catalytic surface area is only valid if the precious metal particles are not too small.

Regarding thermal aging, the catalytic activity is mainly reduced by two effects [16]. The first effect is that sintering will reduce the catalytically active surface, hence the number of available surface sites. As a second effect, the turn over frequency (TOF, also called intrinsic activity) can be affected by the change of the particle diameter. If the particle diameter of the fresh catalyst is already out of the range of structure sensistivity, the aging will only affect the catalytically active surface and the same correlation as for precious metal reduction should be valid. It even makes no difference if the aging process affects not only the particle size but also the morphology of the catalyst, as the number of accesible surface sites is determined by chemisorption measurement.

6. Kinetics and extended model

None of the five DOCs investigated in this paper have particles smaller than 8 nm (Section 3). Hence, the assumption that the catalysts are in the structure insensitive regime is feasible. If the reaction is structure insensitive, the catalyst activity only depends on the number of available surface sites, which can be expressed by the specific platinum surface (Eq. (1)). This is a measurable quantity, which can be determined by e.g. CO-chemisorption measurements.

In the structure insensitive regime the activation energy of the global kinetic model, which is a lumped quantity of contributions from different types of surface sites, is not affected by a change in the catalytically active surface. Only the frequency of the reaction is expected to be influenced. This means that the frequency factor, i.e. the reaction rate constant, should be directly proportional to the catalytically active surface.

$$CO + X \underset{k_1^-}{\overset{k_1^+}{\rightleftharpoons}} COX \tag{6}$$

$$O_2 + 2X \underset{k_2^-}{\overset{k_2^+}{\rightleftharpoons}} 2OX \tag{7}$$

$$COX + OX \xrightarrow{k_3^+} CO_2X + X \tag{8}$$

$$CO_2X \underset{k_4^-}{\overset{k_4^+}{\rightleftharpoons}} CO_2 + X \tag{9}$$

$$r_1 = k_1^+ c_{CO}\theta_X - k_1^- \theta_{CO} \equiv 0 \tag{10}$$

The inhibition term in the global kinetic model originates from adsorption/desorption equilibria [17]. As an example the basic steps for the CO oxidation are given in Eqs. (6)–(9). Application of the equilibrium assumption (e.g. Eq. (10)) and the overall balance of available surface sites for all adsorption/desorption processes results in a set of algebraic equations between the gaseous species and the surface species. If we further assume that the adsorption equilibrium is not coverage dependent, we end up with the classical Langmuir–Hinshelwood reaction scheme and we can find an explicit expression for the surface species. In any case the derived overall reaction rates r_3 for CO oxidation, r_5 for NO oxidation and r_6 for propene oxidation depend only on gas phase concentrations (Eqs. (11)–(13)). The NO oxidation is additionally inhibited by the product [18]. Most DOC models use the rate expressions suggested by Voltz et al. [19]. It is based on an Langmuir–Hinshelwood kinetic approach but the inhibition term is extended by an extra term to fit experimental datas at higher concentrations of CO and HC. As it was possible to reproduce the experimental results over a wide range of concentrations with the pure Langmuir–Hinshelwood inhibition term, we did not extend the inihibition term with the extra terms of Voltz.

$$r_3 = \frac{k_3^* y_{O_2}^a y_{CO}}{\left(1 + K_1^{CO} y_{CO}^q + K_2^{C_3H_6} y_{C_3H_6} + K_3^{NO} y_{NO}\right)^2} \tag{11}$$

$$r_5 = \frac{k_5^* y_{O_2}^{0.5} y_{NO}}{\left(1 + K_5^{NO} y_{NO} + K_5^{NO_2} y_{NO_2}\right)^2} \left(1 - \frac{y_{NO_2}}{y_{O_2}^{0.5} y_{NO} K_{equ}}\right) \tag{12}$$

$$r_6 = \frac{k_6^* \sqrt{y_{O_2}}\, y_{C_3H_6}}{\left(1 + K_6^{CO} y_{CO} + K_6^{C_3H_6} y_{C_3H_6} + K_6^{NO} y_{NO}\right)^2} \tag{13}$$

Reaction rate constant k_i according to Arrhenius:

$$k_i(T) = k_i(573,15K) \exp\left(-\frac{E_{a_i}}{R}\left(\frac{1}{T} - \frac{1}{573,15K}\right)\right)$$

Inhibition term constant K_i^{inhj} according to Arrhenius:

$$K_i^{inhj}(T) = K_i^{inhj}(573,15K) \exp\left(-\frac{E_{a_i}^{inhj}}{R}\left(\frac{1}{T} - \frac{1}{573,15K}\right)\right)$$

In terms of a micro-kinetic view the equilibrium of a component j may also be a function of the surface coverages q_j as shown in Eq. (14) for CO adsorption equilibrium.

$$r_1 = k_1^+ c_{CO}\theta_X - k_1^- \theta_{CO} \exp\left[\frac{\varepsilon_{1,CO}\theta_{CO}}{RT}\right] \tag{14}$$

Taking surface coverage into consideration the algebraic equations are non-linear and no explicit expressions for the surface species can be found. For a global kinetic model this means that

the denomiator of the rate expression must be derived semi-empirically from kinetic measurements and the concentration dependence of the inhibition terms may be different from the prediction of the classical Langmuir–Hinshelwood theory. This is why the self-inhibition of CO in Eq. (11) has an exponent q.

Nevertheless the inhibition term is independent of the total number of surface sites even if we assume that adsorption/desorption is not a totally random process and interaction of various surface species affect the adsorption/desorption equilibrium of species j. As long as the properties of the catalytically active surface are size independent, any inhibition and enhancement effects will have the same influence on small and large catalyst particles.

The only quantities which change with the frequency of a specific reaction are the concentration gradients due to transport resistances between the flowing gas and the catalytically active surface. In the model Eqs. (2) and (3) the external transport resistance is separately accounted for in the mass transfer parameter b, while the internal mass transfer in the washcoat is included in the global kinetics.

If the above assumptions are valid, experimental results with (fresh or aged) catalysts of different active surface area should be described with the same global kinetic models if the respective rate constants are adjusted to the respective surface area. Once the reaction rate of reaction i for a reference catalyst DOC_{ref} is known, the reaction rate for catalyst DOC_x can be predicted by scaling with the specific platinum surface O_{Pt} of both catalysts if the reaction can be treated as structure insensitive.

$$r_i^x = k_i^{ref} \frac{O_{Pt}^x}{O_{Pt}^{ref}} \frac{1}{I_i^2} \prod_{j=1}^{J_{Ed}} (y_j)^{q_i^j} \tag{15}$$

In Fig. 4 the specific platinum surface O_{Pt} measured by chemisorption is shown for the five DOCs under investigation. It can be seen that a reduction in the precious metal loading as well as aging reduced the available active platinum surface.

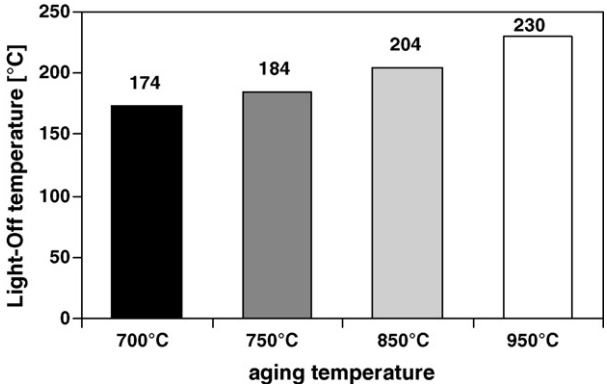

Fig. 5. Light-off temperature for aged catalysts in an adiabatic tubular quartz glass reactor. Feed: 1000 ppm propene in air. Temperature ramp: 10 K/min.

7. Results and discussion

To evaluate the influence of the thermal aging on the dynamic behaviour of the catalysts (e.g. in the cold-start phase of a driving cycle), light-off experiments were achieved. The light-off temperature was determined in an adiabatic quartz tube reactor with 1000 ppm propene in air with a temperature ramp of 10 K/min. The aging resulted in an increase of the light-off temperature of propene as shown in Fig. 5. The results obtained are in accordance with aging experiments reported in the literature [16,20,21].

For model calibration and validation, steady-state experiments obtained in the isothermal flat bed reactor (Section 2.2) were used. Measurements with either CO, propene or NO were realised to verify if all reactions are similarly influenced by aging and changes

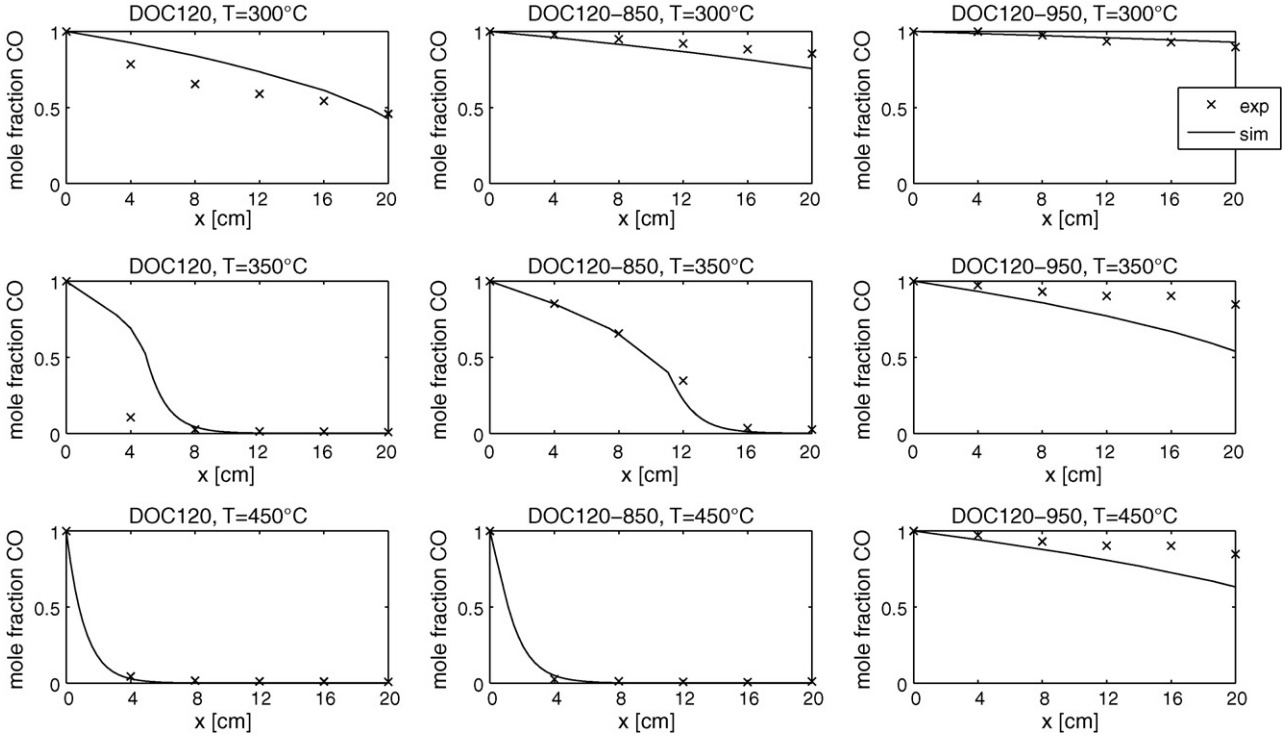

Fig. 6. Axial profiles of CO oxidation for DOC120, DOC120-850 and DOC120-950 at T = 300, 350 and 450 °C with 15,000 ppm CO in the feed. The mole fraction in the plot is normalized by the feed value. For DOC120-850 the kinetic parameters were fitted. For DOC120 and DOC120-950 the parameters found for DOC120-850 were used and only the reaction rate constant was scaled with the specific platinum surface.

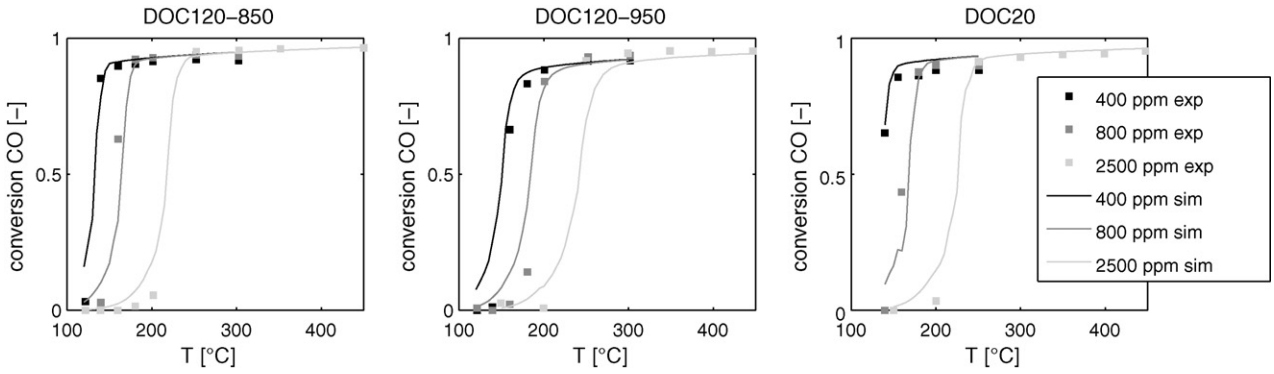

Fig. 7. CO conversion after the first catalyst slice (4 cm), inlet: 400, 800 and 2500 ppm CO. DOC120-850 was fitted and used as basis. For DOC20 and DOC120-950, only the reaction rate constants were scaled with specific platinum surface.

in the precious metal loading. Additionally, mixtures of CO and propene as a more realistic exhaust gas composition were analysed to fit the inhibition terms of the reactions.

7.1. CO oxidation

Experiments were carried out with several CO concentrations (400/800/2500 ppm + 12% O_2 (lean) and 15,000 ppm CO + O_2 (stoichiometric)) between 120 and 450 °C. The DOC120-850 was used as reference catalyst for which the parameters of the global kinetic model are fitted, taking all concentration and temperature variations into account. This ensures that the kinetics are valid over a wide range. As an example, Fig. 6 shows the results of experiment and simulation for 15,000 ppm CO for DOC 120, DOC 120-850 and DOC 120-950. The mole fraction is normalized by the feed value and plotted along the catalyst length *x*. As the catalyst slices in the flat bed reactor have a length of 4 cm, gas compositions are obtained in 4 cm intervals. The negative reaction order of the CO oxidation, which can be seen for DOC120-850 especially at $T = 350$ °C, is well reproduced by the simulation. For the simulation of DOC120 and DOC120-950, the kinetic expression derived for DOC120-850 is used with the only change that the reaction rate is scaled by the ratio of the specific platinum surface according to Eq. (15). Agreement between model prediction and experimental results is quite good.

Due to the large number of experiments, instead of axial profiles, only the conversion after the first or last catalyst slice versus the temperature will be shown subsequently. In Fig. 7, the CO conversion after the first catalyst slice is shown for three concentrations. Again scaling of reaction rates by the specific platinum surface results in a good prediction. Next the approach was applied to the variation of precious metal loading (DOC20 and DOC60). The experimental results can be reproduced quite well (DOC20 in Fig. 7). So the extended model approach suits well for the CO oxidation.

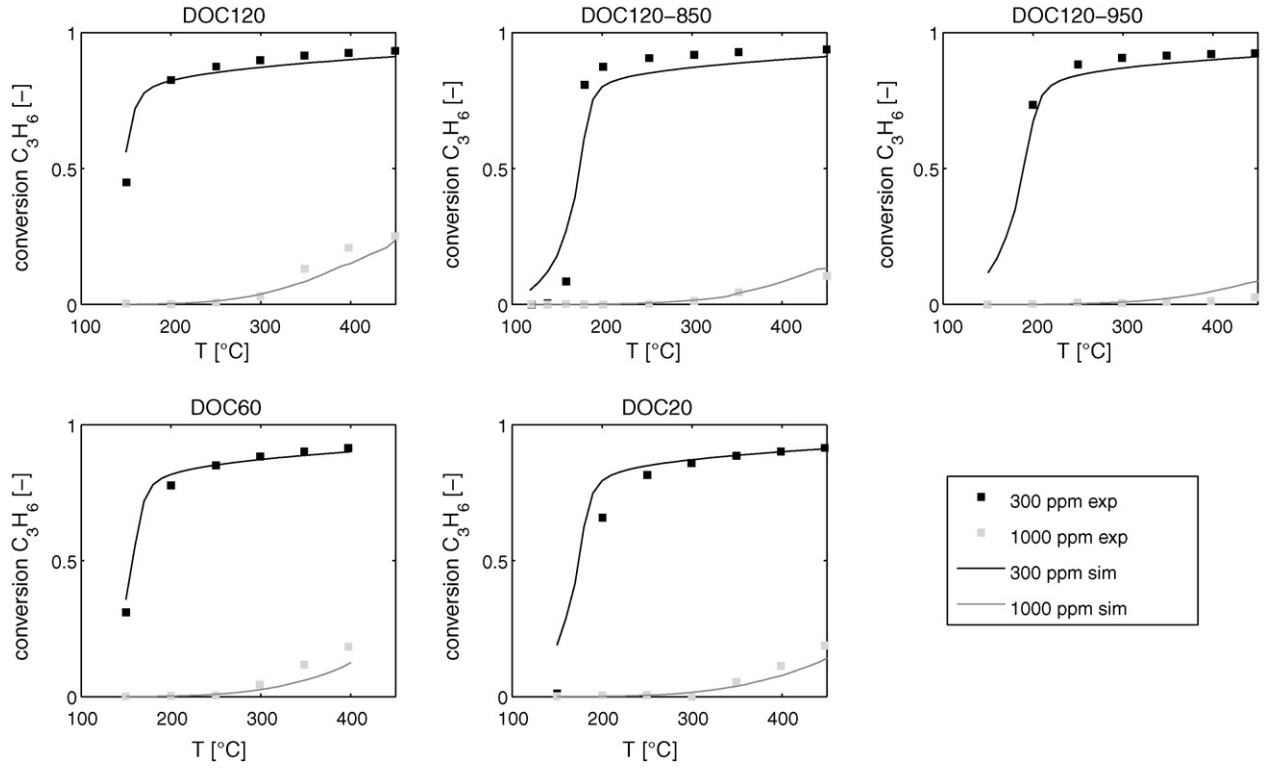

Fig. 8. Propene conversion after the last catalyst slice (20 cm), inlet: 300 ppm and 1000 ppm propene. DOC aging and precious metal variation. DOC120 was fitted and used as basis. For the other catalysts, only the reaction rate constants were scaled with specific platinum surface.

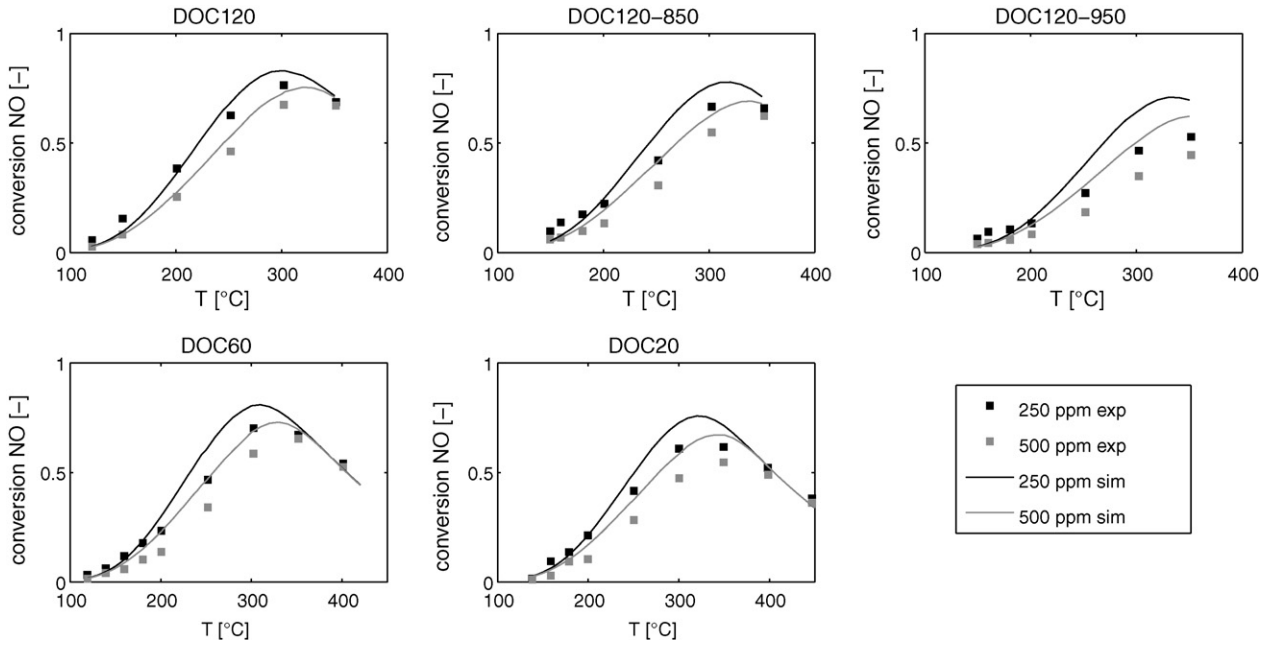

Fig. 9. NO conversion after the last catalyst slice (20 cm), inlet: 250 and 500 ppm NO. DOC aging and precious metal variation. DOC120 was fitted and used as basis. For the other catalysts, only the reaction rate constants were scaled with specific platinum surface.

7.2. Propene oxidation

Next the correlation was verified with the propene oxidation. Here the DOC120 was used as a reference catalyst for the propene oxidation rate. The propene oxidation was examined with 60, 90 and 300 ppm (lean, 12% O_2) and 1000 ppm propene (O_2 stoichiometric) between 120 and 450 °C. Kinetic parameters were fitted against all experimental data. Fig. 8 shows two selected results, namely comparison for 300 and 1000 ppm after the last catalyst slice. It can be seen that scaling of the reaction rate constant with the specific platinum surface O_{Pt} according to Eq. (15) gives a good accordance between the experiments and the simulation.

7.3. NO oxidation

The NO oxidation has been investigated with 250 and 500 ppm NO plus 12% O_2 in the feed. In Fig. 9 the conversion after the last catalyst slice versus the temperature is plotted. The NO conversion is kinetically limited for temperatures below 300 °C. Above 350 °C the NO oxidation is limited by the equilibrium. The parameters of DOC120 were fitted to the experiments. For the other catalysts, the parameters of DOC120 were used by scaling only the reaction rate constant with the specific platinum surface O_{Pt} according to Eq. (15). This approach gives quite acceptable results, but a systematic error occurs in the model prediction. The conversion was underestimated at low temperatures and overestimated at high temperatures. We attribute this to the formation of platinum oxides by the formed NO_2, which has been reported by [22–24]. These oxides are formed at temperatures above 250 °C. If we restrict the experimental results to this temperature range, NO conversion can be predicted well by the model for all five catalysts, adjusted to the DOC120 sample (see Fig. 10). Again, only the reaction rate constant has to be scaled by the specific platinum surface. Experiments on deactivation effects caused by platinum oxide formation are to be published.

7.4. Mixture of CO and propene

In addition, lean mixtures were analysed. As NO/NO_2 is reduzing/oxidizing the platinum and thereby changing the catalysts activity during the experiment, we chose experiments without NO in the feed to show that the correlations work for mixtures as well. For DOC120-850, the inhibition of CO on propene oxidation and vice versa was fitted to four lean mixture experiments (60 ppm propene + 400 ppm CO, 90 ppm propene + 400 ppm CO, 60 ppm propene + 800 ppm CO, 90 ppm propene + 800 ppm CO, each with 12% O_2). The inhibition term was applied for the aged catalysts without change. As an example, experiments with 90 ppm propene and 400 ppm CO are shown for the aging variation (Fig. 11). Similar results have been obtained for other mixtures. This shows that the above approach can also be successfully applied to mixtures.

7.5. Relation of platinum loading and active surface

The three catalysts of the precious metal variation show a linear dependency between the specific platinum surface and the platinum loading in the considered range (Fig. 12). In this case it is even possible to directly use the platinum loading instead of the

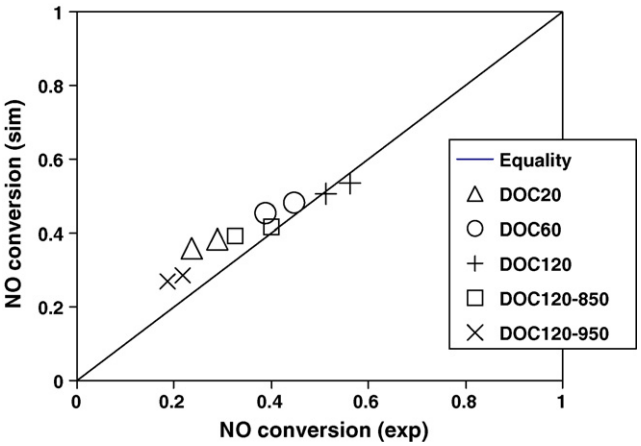

Fig. 10. Parity plot for the oxidation of 250 and 500 ppm NO at 350 °C. The simulated conversion is plotted versus the experimental conversion.

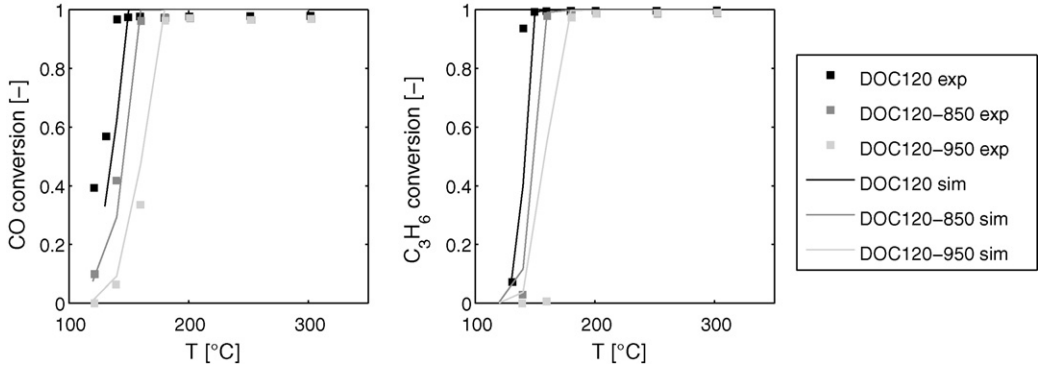

Fig. 11. Experiments with a mixture of 90 ppm propene, 400 ppm CO and 12% O_2 after the last catalyst slice (20 cm), DOC aging variation. DOC120-850 was fitted and used as basis. For the other catalysts, only the reaction rate constants were scaled with specific platinum surface. The inhibition term parameters are the ones found for DOC120-850.

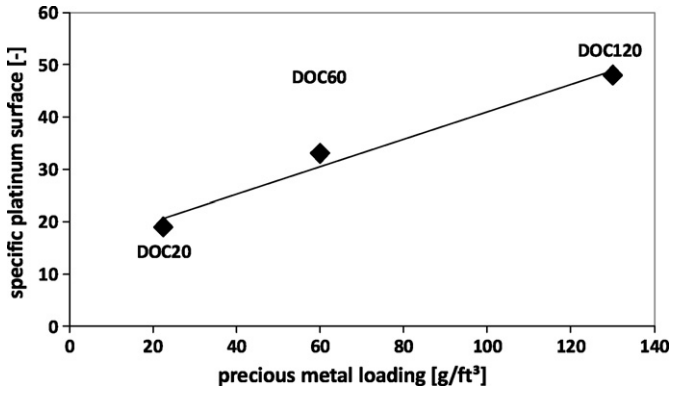

Fig. 12. Measured specific platinum surface versus precious metal loading.

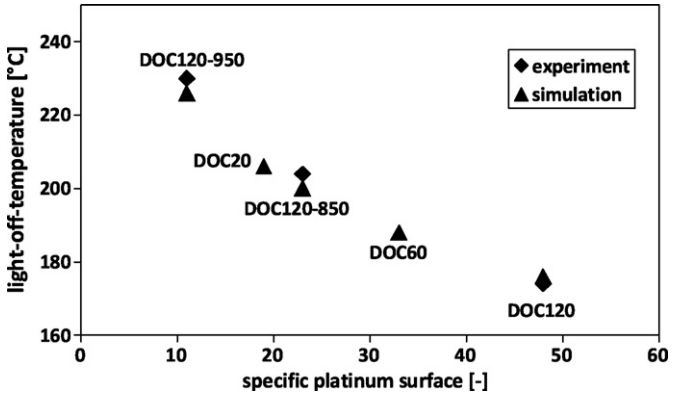

Fig. 13. Specific platinum surface versus light-off temperature.

active platinum surface as input parameter for the simulation. This justifies that in literature the reaction rate constant of the NO oxidation depends linearly on the precious metal loading [25]. It should be noted that such a dependency is only valid if the reaction is structure insensitive.

7.6. Relation of platinum active surface and light-off temperature

It is even possible to determine the active precious metal surface of a given catalyst by a simple light-off experiment instead of CO chemisorption. In Fig. 13 the experimental determined light-off temperature (Fig. 5) is plotted versus the specific platinum surface measured by chemisorption (Fig. 4). Additionally, the light-off temperature was adiabatically simulated with the kinetic model scaled by the specific platinum surface. For DOC120 and the aged catalysts the comparison with the measurements shows a good accordance. This means that one can fit the specific platinum surface with a light-off experiment and use it for scaling the entire kinetic model.

8. Summary

In this paper, five DOCs ($Pt–Al_2O_3$) with different platinum loadings and aging steps were characterized regarding platinum particle diameter, active surface area and conversion behaviour for CO, propene and NO oxidation. As there are no platinum particles smaller than 8 nm, all catalysts are in the structure insensitive regime. In this case the catalyst activity is shown to be directly proportional to the catalytic active surface area, which was determined by chemisorption measurements. This means that only the rate constants of the respective kinetics have to be adjusted to the active surface area, if the catalyst is aged or the precious metal loading varies. It is shown that this approach works quite well for a global model based on generalized Langmuir–Hinshelwood kinetics.

It has to be mentioned that the here used $Pt–Al_2O_3$ DOC is a very simple model catalyst. It is not clear if the correlation for the catalysts activity after aging could be transferred to commercial catalyst systems, which contain additives for stabilization, zeolites for light-off improvement and possibly more than one precious metal species so that alloys might be formed. This is the topic of ongoing research.

Acknowledgements

The authors would like to gratefully acknowledge the Forschungsvereinigung Verbrennungskraftmaschinen (FVV e.V.) for the financial support and Umicore AG&Co.KG for providing the catalysts. The authors are indebted to Prof. Dr. Deutschmann and Willi Boll (ITCP, University Karlsruhe) for providing their experimental results on the surface characteristics of the catalysts tested.

References

[1] W. Hauptmann, A. Drochner, H. Vogel, M. Votsmeier, J. Gieshoff, Topics in Catalysis 42–43 (2007) 157–160.
[2] C. Sampara, E. Bissett, M. Chmielewski, D. Assanis, Industrial & Engineering Chemistry Research 46 (2007) 7993–8003.
[3] J. Koop, O. Deutschmann, Applied Catalysis B: Environmental 91 (2009) 47–58.
[4] L. Olsson, R. Blint, E. Fridell, Industrial & Engineering Chemistry Research 44 (2005) 3021–3032.
[5] V. Schmeißer, U. Tuttlies, G. Eigenberger, Topics in Catalysis 42–43 (2007) 77–81.
[6] S. Oh, J. Cavendish, Industrial & Engineering Chemistry Product Research and Development 21 (1982) 29–37.
[7] T. Wang, S. Baek, J.-H. Lee, Industrial & Engineering Chemistry Research 47 (2008) 2528–2537.
[8] Y.-D. Kim, W.-S. Kim, Industrial & Engineering Chemistry Research 48 (2009) 6579–6590.

[9] V. Schmeißer, J. Perez, U. Tuttlies, G. Eigenberger, Topics in Catalysis 42–43 (2007) 15–19.
[10] J. Anderson, M. Fernandez Garcia, Supported Metals in Catalysis, Imperial College Press, 2005.
[11] S. Wanke, P. Flynn, Catalysis Reviews 12 (1975) 93–135.
[12] P. Flynn, S. Wanke, Journal of Catalysis 34 (3) (1974) 390–399.
[13] R. van Hardeveld, F. Hartog, Surface Science 15 (1969) 189–230.
[14] R. van Santen, Accounts of Chemical Research 42 (2009) 57–66.
[15] F. Gracia, L. Bollmann, E. Wolf, J. Miller, A. Kropf, Journal of Catalysis 220 (2003) 382–391.
[16] J Yang, V. Tschamber, D. Habermacher, F. Garin, P. Gilot, Applied Catalysis B: Environmental 83 (2008) 229–239.
[17] I. Chorkendorff, J. Niemantsverdriet, Concepts of Meodern Catalysis and Kinetics, Wiley-VCH Verlag GmbH & Co.KGaA, 2007.
[18] S. Mulla, N. Chen, W. Delgass, W. Epling, F. Ribeiro, Catalysis Letters 100 (2005) 267–270.
[19] S. Voltz, C. Morgan, D. Liederman, S. Jacob, Industrial & Engineering Chemistry Product Research and Development 12 (1973) 294–301.
[20] A.K. Datye, Q. Xu, K. Kharas, J. McCarty, Catalysis Today 111 (2006) 59–67.
[21] Y. Nagai, T. Hirabayashi, K. Dohmae, N. Tagagi, T. Minami, H. Shinjoh, S. Matsumoto, Journal of Catalysis 242 (2006) 103–109.
[22] J. Després, M. Elsener, M. Koebel, O. Kröcher, B. Schnyder, A. Wokaun, Applied Catalysis B: Environmental 50 (2004) 73–82.
[23] L. Olsson, E. Fridell, Journal of Catalysis 210 (2002) 340–353.
[24] W. Hauptmann, M. Votsmeier, J. Gieshoff, A. Drochner, H. Vogel, Applied Catalysis B: Environmental 93 (2009) 22–29.
[25] D. Chatterjee, T. Burkhardt, T. Rappe, A. Güthenke, M. Weibel, SAE technical papers 2008-01-0867 (2008).